

Video Article

# Experimental Protocol to Investigate Particle Aerosolization of a Product Under Abrasion and Under Environmental Weathering

Neeraj Shandilya<sup>1,2</sup>, Olivier Louis Le Bihan<sup>1</sup>, Christophe Bressot<sup>1</sup>, Martin Morgeneyer<sup>2</sup>

<sup>1</sup>Direction des Risques Chroniques, Institut National de l'Environnement Industriel et des Risques (INERIS)

<sup>2</sup>Génie des Procédés Industriels, Université de Technologie de Compiègne (UTC)

Correspondence to: Martin Morgeneyer at [martin.morgeneyer@utc.fr](mailto:martin.morgeneyer@utc.fr)

URL: <https://www.jove.com/video/53496>

DOI: [doi:10.3791/53496](https://doi.org/10.3791/53496)

Keywords: Engineering, Issue 115, Nanomaterials, Particles, Nanosafety-by-design, Product design, Abrasion, Weathering, Emission, Aerosol. Physics

Date Published: 9/16/2016

Citation: Shandilya, N., Le Bihan, O.L., Bressot, C., Morgeneyer, M. Experimental Protocol to Investigate Particle Aerosolization of a Product Under Abrasion and Under Environmental Weathering. *J. Vis. Exp.* (115), e53496, doi:10.3791/53496 (2016).

## Abstract

The present article presents an experimental protocol to investigate particle aerosolization of a product under abrasion and under environmental weathering, which is a fundamental element to the approach of nanosafety-by-design of nanostructured products for their durable development. This approach is basically a preemptive one in which the focus is put on minimizing the emission of engineered nanomaterials' aerosols during the usage phase of the product's life cycle. This can be attained by altering its material properties during its design phase without compromising with any of its added benefits. In this article, an experimental protocol is presented to investigate the nanosafety-by-design of three commercial nanostructured products with respect to their mechanical solicitation and environmental weathering. The means chosen for applying the mechanical solicitation is an abrasion process and for the environmental weathering, it is an accelerated UV exposure in the presence of humidity and heat. The eventual emission of engineered nanomaterials is studied in terms of their number concentration, size distribution, morphology and chemical composition. The purpose of the protocol is to study the emission for test samples and experimental conditions which are corresponding to real life situations. It was found that the application of the mechanical stresses alone emits the engineered nanomaterials' aerosols in which the engineered nanomaterial is always embedded inside the product matrix, thus, a representative product element. In such a case, the emitted aerosols comprise of both nanoparticles as well as microparticles. But if the mechanical stresses are coupled with the environmental weathering, the experimental protocol reveals then the eventual deterioration of the product, after a certain weathering duration, may lead to the emission of the free engineered nanomaterial aerosols too.

## Video Link

The video component of this article can be found at <https://www.jove.com/video/53496/>

## Introduction

With a rapid maturity in the nanotechnology, its advancement is driven by rapid commercialization of products containing *Engineered Nanomaterials* (ENM) with remarkable properties. As described by Potocnick<sup>1</sup> in the article 18(5) of Regulation 1169/2011, issued by the European Commission, ENM can be defined as "any intentionally manufactured material, containing particles, in an unbound state or as an aggregate or as an agglomerate and where, for 50% or more of the particles in the number size distribution, one or more external dimensions is in the size range 1 nm to 100 nm". Moreover, the products containing ENM, either in their solid bulk or on their solid surfaces or in their liquid suspensions, can be termed as *Nanostructured products*. Different types of ENM with different formulations and functionalizations are used in such products according to the nature of application and budget. The products can be in the form of coatings, paints, tiles, house bricks, concrete etc.

As far as the research is concerned, one may also find enormous number of publications on the innovations that have been accomplished through nanotechnology. Despite this enormous research, the appealing traits of ENM are under probe for potential health or environmental dangers due to their tendency to get released or emitted in air in the form of aerosols during the use or processing of the nanostructures products (for example Oberdorster *et al.*<sup>2</sup>, Le Bihan *et al.*<sup>3</sup> and Houdy *et al.*<sup>4</sup>). Kulkarni *et al.*<sup>5</sup> defines an aerosol as the suspension of solid or liquid particles in the gaseous medium. Hsu and Chein<sup>6</sup> have demonstrated that during the use or processing of a nanostructured product, a nanostructured product is subjected to various mechanical stresses and *environmental weathering* which facilitate such an emission.

According to Maynard<sup>7</sup>, upon exposure, these aerosols of ENM may interact with human organism through inhalation or dermal contacts and get deposited inside the body which consequently may cause various detrimental effects, including the carcinogenic ones. Thus, a thorough understanding of the ENM emission phenomenon is of paramount importance given the unprecedented use of nanostructured products, as mentioned by Shatkin *et al.*<sup>8</sup>. This may not only help in avoiding unanticipated health related complications arising from their *exposure* but also in encouraging public confidence in nanotechnologies.

Nevertheless, the exposure related problem has now started getting attention by the research community and has been recently highlighted by various research units throughout the world (for example, Hsu and Chein<sup>6</sup>, Göhler *et al.*<sup>9</sup>, Allen *et al.*<sup>10</sup>, Allen *et al.*<sup>11</sup>, Al-Kattan *et al.*<sup>12</sup>, Kaegi *et al.*<sup>13</sup>, Hirth *et al.*<sup>14</sup>, Shandilya *et al.*<sup>15, 31, 33</sup>, Wohlleben *et al.*<sup>16</sup>, Bouillard *et al.*<sup>17</sup>, Ounoughene *et al.*<sup>18</sup>). Considering the large scale deployment of nanostructured products in the commercial markets, the most effective approach to tackle the problem would be a preemptive one. In such an approach, a product is designed in such a way that it is "nanosafe-by-design" or "Design for safer Nanotechnology" (Morose<sup>19</sup>) *i.e.*, low emissive. In other words, it maximizes their benefits in problem solving during its use while emitting a minimum amount of aerosols in the environment.

To test the nanosafety-by-design during the usage phase of a nanostructured product, the authors present an appropriate experimental methodology to do so in the present article. This methodology consists of two types of solicitations: (i) *mechanical* and (ii) *environmental* which aim at simulating the real life stresses to which the nanostructured product, a masonry brick, is subjected to during its usage phase.

(i) A linear abrasion apparatus which simulates the mechanical solicitation. Its original and commercial form, as shown in **Figure 1A**, is referenced in numerous internationally recognized test standards like ASTM D4060<sup>20</sup>, ASTM D6037<sup>21</sup> and ASTM D1044<sup>22</sup>. According to Golanski *et al.*<sup>23</sup>, due to its robust and user-friendly design, its original form is already being used widely in industries for analyzing the performance of products like paint, coating, metal, paper, textile, etc. The stress being applied through this apparatus corresponds to the typical one applied in a domestic setting, for example, walking with shoes and displacement of different objects in a household (Vorbau *et al.*<sup>24</sup> and Hassan *et al.*<sup>25</sup>). In **Figure 1A**, a horizontally displacing bar moves the standard abrasant in a to and fro motion over the sample surface. The abrasion wear occurs at the contact surface due to the friction at the contact. The magnitude of the abrasion wear can be varied by varying the normal load ( $F_N$ ) which acts at the top of the abrasant. By changing the type of the abrasant and normal load value, one may vary the abrasiveness and hence the mechanical stress. Morgeneyer *et al.*<sup>26</sup> have pointed out that the stress tensor to be measured during abrasion is composed of normal and tangential components. The normal stress is the direct result of the normal load, *i.e.*, of  $F_N$  whereas the tangential stress is the result of the tangentially acting friction process, measured as force ( $F_T$ ) and it acts parallel or anti-parallel to the direction in which abrasion takes place. In the original form of this abrasion apparatus, one cannot determine  $F_T$ . Therefore, the role of the mechanical stresses during the aerosolization of ENM cannot completely be determined. To eradicate this limitation, as described in details by Morgeneyer *et al.*<sup>26</sup>, we have (a) modified it by replacing the already installed horizontal steel bar by a replica in aluminum 2024 alloy and (b) mounted a strain gauge on the top surface of this replicated aluminum alloy bar. This is shown in **Figure 1B**. This strain gauge has 1.5 mm of active measuring grid length and 5.7 mm of measuring grid carrier length. It is made of a constantan foil having 3.8  $\mu\text{m}$  of thickness and  $1.95 \pm 1.5\%$  of gauge factor. A proper measurement of the mechanical stresses are ensured through a dynamic strain gauge amplifier which is connected in series to the strain gauge, thus allowing a reliable measurement of the strain produced in the gauge. The data transmitted via amplifier is acquired using data acquisition software.

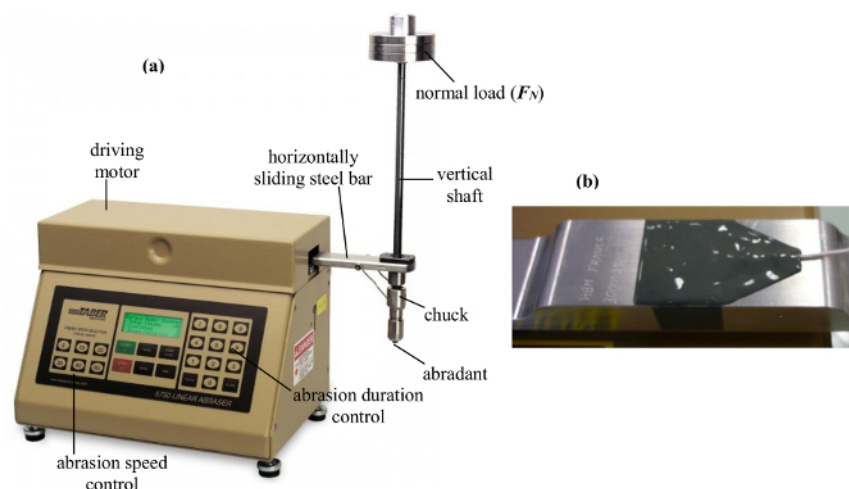


**Figure 1. Abrasion Apparatus and Strain Gauge.** The commercial standard form of the Taber abrasion apparatus (**A**) with abrasion speed, duration and stroke length controls. The originally mounted steel bar was replaced by an aluminum bar and was further equipped with a strain gauge (**B**) to measure the tangential force ( $F_T$ ). [Please click here to view a larger version of this figure.](#)

In the **Figure 2**, the complete experimental set-up is shown where this modified Taber abrasion apparatus is placed under the conformity of a nanosecured work post. A particle free air is constantly circulating inside this work post at a flow rate of 31,000 l/min. It has a particle filter efficiency of 99.99% and has already been successfully employed by Morgeneyer *et al.*<sup>27</sup> in various nanoparticles' dustiness tests.

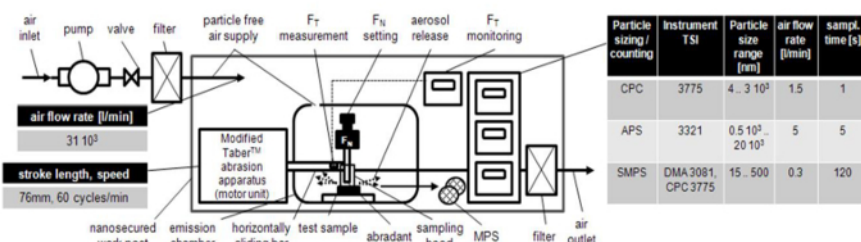


**Figure 2. Experimental Set-up (Shandilya *et al.*<sup>31</sup>).** A nanosecured work facility to carry out the abrasion tests and real time characterization (both qualitative and quantitative) of the generated aerosol particles. A small fraction of the particle free air passes through a slot inside the emission chamber to eliminate its background particles number concentration. [Please click here to view a larger version of this figure.](#)

The motor of the abrasion apparatus is kept outside and its linearly sliding part is kept inside a self-designed *emission test chamber*, with dimensions, 0.5 m × 0.3 m × 0.6 m, (details in Le Bihan *et al.*<sup>28</sup>). It helps in preventing the abrasion apparatus' motor emissions from interfering in the test results. The sampling of the generated aerosol particles is done inside the proximity of a radial symmetric hood (volume of 713 cm<sup>3</sup>). By employing such a hood, the aerosol particles losses due to their deposition on the surfaces can be minimized. The other advantage includes increase in the aerosol particles number concentration due to a relatively lower volume of the hood with respect to the emission test chamber. Thanks to this set up, a real time characterization and analysis of the particle aerosols getting generated during the abrasion wear can be done experimentally in terms of their *number concentrations*, *size distributions*, *elemental compositions* and *shapes*. According to Kulkarni *et al.*<sup>5</sup>, the number concentration of ENM aerosols particles can be defined as "the number of ENM present in unit cubic centimeter of air". Similarly, the size distribution of ENM aerosols is "the relationship expressing the quantity of an ENM property (usually number and mass concentrations) associated with particles in a given size range".

A particle Counter (measurable size range: 4 nm to 3 µm) measures the aerosol particles number concentration (**PNC**). The particle sizers (measurable size range: 15 nm - 20 µm) measure the particle size distribution (**PSD**). An aerosol particles sampler (described in details by R'mili *et al.*<sup>30</sup>) is used for the particle collection through filtration technique on a porous copper mesh grid which can be used later in Transmission Electron Microscope (TEM) for various qualitative analyses of the released particles.

(ii) The environmental solicitation can be simulated through accelerated artificial weathering in a weathering chamber, shown in **Figure 3**. As shown by Shandilya *et al.*<sup>31</sup>, the weathering conditions can be kept in conformity with the international standards or be customized depending upon the type of simulation. The UV exposure is provided via xenon arc lamp (300 – 400 nm) installed with an optical radiation filter. The action of rain is simulated by spraying deionized and purified water onto them. A reservoir is placed beneath the test samples to collect the runoff water. The collected water or leachate can be used later to perform the ENM leaching analysis.



**Figure 3. Weathering Chamber.** The commercial form of the Suntest XLS+ weathering chamber contains a stainless steel hood inside which the nanocoated samples are placed. The water reservoir is placed beneath the hood which is the source of the water to be sprayed inside the hood. [Please click here to view a larger version of this figure.](#)

## Protocol

NOTE: The technique presented in the Protocol here is not only limited to the presented test samples but can be used for other samples as well.

### 1. Artificial Weathering [CEREGE Platform, Aix en Provence]

1. Take a 250 ml sample of the deionized and purified water to be sprayed in a beaker. Immerse the tip of the water conductivity meter into the water. Note the water conductivity. Repeat the process and note the water conductivity each time.  
NOTE: According to the ISO 16474<sup>32</sup>, it should never be higher than 5 µS/cm.
2. After measuring the conductivity, connect the water source to the reservoir of the weathering chamber present underneath the stainless steel hood (shown in **Figure 3**).
3. Connect the overflow spout on the back of the chamber to a drain opening through a hose pipe.
4. Place the nanocoating samples to weather into the stainless steel hood and close the door. To enable a statistical evaluation of the results, use a minimum of three identical nanocoating and reference samples.
5. On the digital console, present on the front of the weathering chamber, select a 2 hr cycle composed of 120 min of UV light, 102 min dry and 18 min water spray.
6. Enter the number of cycles equal to 2658 which corresponds to 7 months.

7. Choose the irradiance level of the xenon arc lamp equal to  $60 \pm 5 \text{ W/m}^2$ .
8. Set the ambient temperature at  $38^\circ\text{C}$ .
9. Start the weathering test by pressing the LAUNCH button on the console.

## 2. Abrasion and ENM Aerosols Characterization [INERIS S-NANO Platform, Verneuil]

NOTE: Before using, pre-verify the particle aerosol characterizing instruments on a calibration bench of INERIS S-NANO Platform which comprises of separate and already installed reference counter parts. By following a specific protocol, ensure that the instruments are working properly.

1. Assemble all the units and instruments shown in the experimental set-up and make the necessary connections as shown in **Figure 2** (details on the units and setting up of instruments are provided in Shandilya *et al.*<sup>33</sup>).
2. Switch on the circulation of the particle free air inside the nanosecured workpost by pressing the FLUX ON button.
3. Make this particle free air to pass through the emission test chamber by opening the chamber and keeping it open inside the nanosecured work post.
4. To set up the experiment, connect the particle counter directly to the emission test chamber to measure the instantaneous number concentration of the particles inside the chamber. Observe the concentration value directly on the display counter.
5. While the particle free air is passing through the chamber, continue to monitor this instantaneous number concentration value until it drops to zero. In this way, ensure that the chamber is free of any background particle.
6. In the meantime, chamfer the edges of the standard cylindrically shaped abrasant by gently turning its one end in a to and fro motion inside the slot of a tool provided with the abrasion apparatus.
7. Using a digital balance with a measurement precision of at least  $0.001 \text{ g}$ , weigh the abrasant and sample to be abraded.
8. Once done, fix the chamfered abrasant to the vertical shaft of the abrasion apparatus through a chuck present at its bottom.
9. Place the nanostructured product to be abraded gently beneath the fixed abrasant and firmly fix its position on the mounting system.
10. Open the aerosol sampler and, by using a tweezer, place a copper mesh grid inside the slot with its brighter side upwards. Put a circular ring over the grid to fix it.
11. Close the sampler and connect it to a pump via a filter on one end (*i.e.*, towards darker side of the grid) and to the particle source on the other end (*i.e.*, towards brighter side of the grid). Mount the required normal load on the vertical shaft using the dead weights.
12. Through the particle counter, check if the background particles concentration inside the open chamber has dropped to zero. If not, wait for it. If yes, close the door of the emission test chamber.
13. Via the digital consoles on the instruments, manually set the flow rates of the particle counter and the sizers as follows: CPC-  $1.5 \text{ l/min}$ ; SMPS-  $0.3 \text{ l/min}$ ; APS-  $5 \text{ l/min}$
14. Set the total sampling duration at 20 min for all these three instruments. Set the abrasion duration and speed equal to 10 min and 60 cycles per minute respectively in the abrasion apparatus.
15. Connect the strain gauge to the dynamic strain gauge amplifier. Connect the dynamic strain gauge amplifier to the computer which shall be used for the data acquisition using software installed in it.
16. Open the software.
17. Click NEW DAQ PROJECT to open a new data acquisition file.
18. Stop the option for live data acquisition by clicking LIVE UPDATE
19. Click 0 EXECUTE to set the reference signal value equal to zero.
20. Switch back on the live data acquisition by clicking LIVE UPDATE.
21. Click VISUALIZATION to choose the real time graphical mode of data representation.
22. Click NEW to open the templates.
23. Choose the option SCOPE PANEL, for example.
24. Start the data acquisition in the particle counters and sizers at once.
25. After a delay of approx. 5 min, start the abrasion.
26. Click START in the data acquisition software window to acquire the strain gauge signals corresponding to the ongoing abrasion.
27. After 2 min, switch on the pump connected to the MPS.
28. Keep the pump running for 2 - 4 min depending upon the quantity of the emission of the aerosol particles. NOTE: The number of aerosol particles sampled using MPS should be optimal in number *i.e.*, neither too scarce nor too surplus which might prevent a thorough microscopic analysis.
29. Once the abrasion stops, switch off the data acquisition by clicking STOP.
30. Save the acquired data by clicking SAVE DATA NOW.
31. After the counter and sizers stop acquiring data, open the emission test chamber and weigh again the abrasant and abraded nanostructured product.
32. Continue the entire process for every abrasion test.
33. Once the abrasion tests, once again verify the three particle aerosol characterizing instruments are on the calibration bench of INERIS S-NANO Platform.

## 3. TEM Analysis of the Liquid Suspensions- Drop Deposition Technique [INERIS Calibration Platform, Verneuil]

1. Prepare a 1% volume diluted aqueous solution of the liquid suspension (*i.e.*, the 'paint') by adding 1 part of the coating suspension in 99 parts of the filtered and de-ionized water.
2. Open the cover of the glow discharge machine
3. Set the following operating conditions:  $0.1 \text{ mbar}$ ,  $45 \text{ mA}$ , 3 min duration.
4. In order to make a TEM copper mesh grid hydrophilic by its plasma treatment, put it on the metal stand. Close the cover and start the motor. After 3 min, it stops automatically.

- Take out the hydrophilic turned mesh grid using a tweezer. Place it gently with its brighter side up. Deposit a drop of the diluted solution (8  $\mu$ l approx.) onto the hydrophilic mesh grid using a syringe.
- Dry the mesh grid in a closed chamber so that the water content gets evaporated and the constituent particles rest deposited on the grid. Make sure that the mesh grid doesn't get charged with the stray particles which can be easily identified as circular or strand shapes which are characteristic of oil or soot particles.
- Once ready, put the grid in the TEM probe and carry out the microscopic analysis. [electron accelerating voltage 120 kV, cf<sup>31</sup>].
- If the grid appears too laden with particles to analyze, lower the dilution percentage and volume of the deposited drop. The maximum volume an operator is able to deposit is approximately equal to 12  $\mu$ l.

## Representative Results

### Test Samples

The protocols presented in the article were applied to three different commercial nanostructured products. A focus is put here on the details of the experimental approach:

(a) alumino-silicate brick reinforced with TiO<sub>2</sub> nanoparticles, (11 cm x 5 cm x 2 cm). It finds its frequent application in constructing façades, house walls, wall tiles, pavements etc. Its material properties along with a scanning electron microscope image are shown in **Table 1** and **Figure 4** respectively.

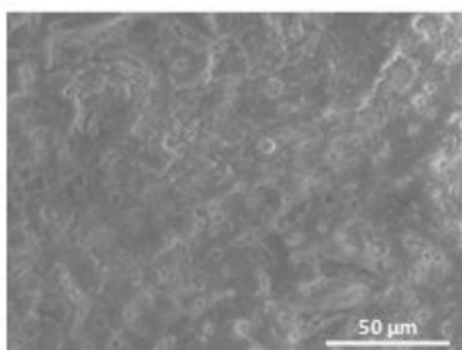


**Figure 4. SEM Image of the Nanostructured Alumino-silicate Brick (Shandilya et al.<sup>33</sup>).** A rough surface with the micro-sized craters or surface asperities can be observed in the image. These surface asperities interact with the abradant during abrasion. [Please click here to view a larger version of this figure.](#)

Properties	Value
Composition	Al, Si, Ca, Ti
rms roughness	7 $\mu$ m
Average primary particle size of TiO <sub>2</sub>	< 20 nm
Elastic modulus	20 Gpa (approx.)
Poisson's ratio	0.2
Vickers Hardness	800 (approx.)

**Table 1: Material Properties of the Nanostructured Alumino-silicate Brick.**

(b) Photocatalytic nanocoatings consisting of anatase titanium dioxide nanoparticles with a PMMA and alcoholic base as dispersants respectively. The Transmission Electron Microscope (TEM) analysis of the two nanocoatings, shown in **Figures 5 (A)** and **(B)**, reveal average TiO<sub>2</sub> particle size equal to  $8 \pm 4$  nm in the former case while  $25 \pm 17$  nm in the latter. Also, two distinct phases contributed by the dispersant (in grey color) and incorporated TiO<sub>2</sub> nanoparticles (in pitch black color) can also be observed. The volume percentages of titanium dioxide nanoparticles in the two nanocoatings are same and equal to 1.1%. The Energy dispersive X-ray analysis (EDX) of the elemental composition of the two nanocoatings, obtained after following the protocol for the drop deposition technique, show similar observations i.e., C (60 to 65% in mass), O (15 to 20% in mass) and Ti (10 to 15% in mass). It should be noted that both nanocoatings are manufactured specifically for applications on external surfaces of the buildings which are generally porous like brick, concrete, etc. Therefore, the substrate chosen for the nanocoating application was a commercial plain masonry brick (11 cm x 5 cm x 5 cm).



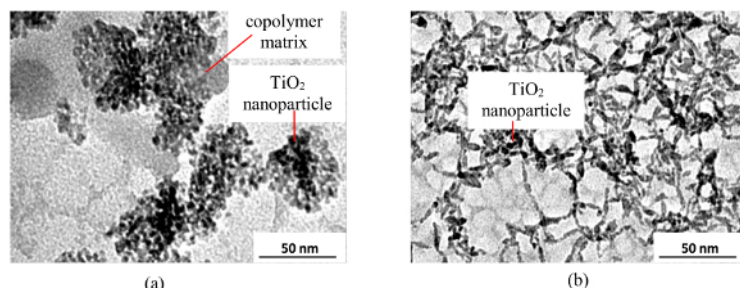


**Figure 5. TEM Image of the Nanoparticles Present in the Nanocoatings with (A) PMMA and (B) Alcoholic Base as Dispersants Respectively (Shandilya *et al.*<sup>33</sup>).** Apart from the different constituent nanoparticles sizes of the two nanocoatings, their individual morphologies are also different *i.e.*, cloud like structure for the former while stranded for the latter. [Please click here to view a larger version of this figure.](#)

(c) Transparent glaze additive consisting of nanoparticles of  $\text{CeO}_2$  having a primary size of 10 nm. It is dispersed in the glaze with 1.3% volume percentage. Such glaze is generally applied on externally lying painted wooden surfaces to impart protection towards their eventual discoloration and weathering with time. In **Figures 6A and B**, TEM image and elemental composition analysis of a sample drop are shown respectively.

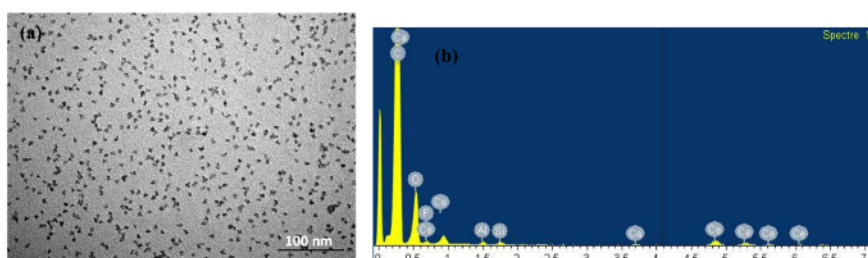


**Figure 6: TEM Image and Elemental Composition Analysis of a Sample Drop.** TEM image (A) and elemental composition analysis (B) of a sample drop are shown [Please click here to view a larger version of this figure.](#)

### Emission from the Nanostructured Brick

The evolution of the total worn mass of the nanostructured brick ( $M_t$ ) during abrasion is shown with respect to  $F_N$  in **Figure 7**. For each value of  $F_N$ , the abrasion test has been repeated thrice. This evolution appears to follow a linear path up to  $F_N = 10.5$  N after which it unexpectedly increases for the higher loads. The standard deviations, measured in the values of the worn mass, range from 0 to 0.023 g. The worn mass of the abradant during each abrasion test was less than 2% that of the brick, therefore negligible.

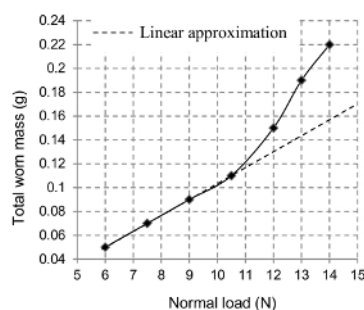


**Figure 7. Wear mass as a function of normal load.** The total worn mass of the brick increases monotonously during its abrasion with constantly increasing normal load (Shandilya *et al.*<sup>33</sup>) [Please click here to view a larger version of this figure.](#)

In **Figure 8**, the unimodal PSD of the emitted aerosol particles are shown for different values of  $F_N$ . For each value, the abrasion test has been repeated thrice. With an increasing  $F_N$ , the mode of the PSD is also increasing. However, beyond 10.5 N, the number concentration peak or the maximum particle number concentration remains stagnant at  $\sim 645 \text{ cm}^{-3}$ .

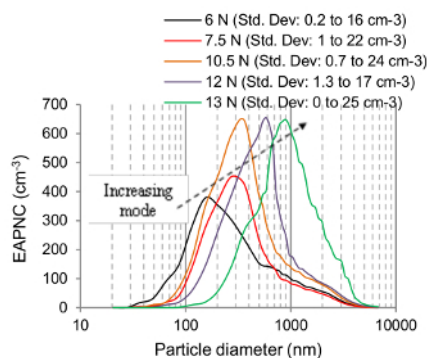


**Figure 8. Aerosol Particles Size as a Function of Normal Load.** The modal size of the particle size distribution (PSD) curves of the emitted aerosol particles increases with normal load (Shandilya *et al.*<sup>33</sup>) [Please click here to view a larger version of this figure.](#)

In **Figure 9A**, the evolution of the total PNC is shown with respect to  $F_N$ . For the particles having sizes in the range of 20–500 nm, it appears to increase up to 10.5 N after which it starts decreasing. For 0.5–20  $\mu\text{m}$  size range, it increases continuously. However, it seems to approach a constant value beyond 10.5 N. However, the behavior of total PNC with respect to the increasing  $F_T$ , shown in **Figure 9B** is different as it increases monotonously. A similar observation can be observed for the PSD modes too.

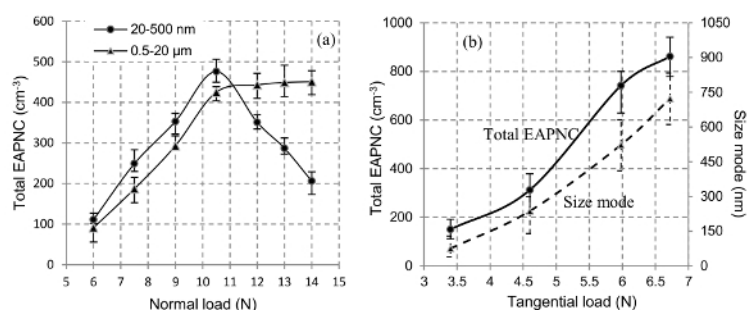


**Figure 9. Emitted Aerosol Particles.** (A) Total emitted aerosol particles number concentration (PNC) of the aerosol particles as a function of normal load (Shandilya *et al.*<sup>34</sup>) (B) Total PNC and PSD mode as a function of tangential load [Please click here to view a larger version of this figure.](#)

For the TEM analysis of the sampled aerosol particles which were collected on a mesh grid during the abrasion at 4 different values of  $F_N$ , the sizes of 50 different aerosol particles were measured for each grid, and their average sizes were determined in each case. **Table 2** shows the average values. A clear increase in the average size of the sampled aerosol particles can be seen with the increasing  $F_N$ .

Normal load (N)	Average aerosol particle size ( $\mu\text{m}$ )
6	$0.2 \pm 0.1$
9	$0.9 \pm 0.3$
10.5	$3 \pm 0.7$
13	$5 \pm 0.6$

**Table 2: Average Aerosol Particle Size of the Sampled Aerosol Particles at Different Values of  $F_N$ .**

### Emission From the Photocatalytic Nanocoatings

To test the emission of aerosol particles from the photocatalytic nanocoatings, abrasion tests of their weathered and non-weathered test samples were done. The results pertaining to their non-weathered samples are presented first. The PNC curves obtained when the 4 layered nanocoatings' test samples were abraded under a normal load of 6 N are shown in the **Figures 10A**. The test was repeated thrice under same conditions. For uncoated reference, the repetition was done on the same brick. In the **Figure 10A** the abrasion starts at  $t = 240$  sec and ends at  $t = 840$  sec. Before and after this time interval ( $t = 0$  to  $240$  sec), the system is idle. The nanocoating with alcoholic base seems to impart no difference on the PNC when it is compared with the uncoated reference. The two have almost the same PNC levels. Since the nanocoating probably gets rubbed off completely without providing any resistance, the PNC attains its maximum value ( $\approx 200 \text{ cm}^{-3}$ ) soon after the abrasion starts. The standard deviation ranges from 5 to  $16 \text{ cm}^{-3}$ . For the nanocoating with PMMA, the PNC is initially low ( $\approx 14 \text{ cm}^{-3}$ ) due to a probable resistance of the nanocoating against abrasion. However, this resistance continues up to a certain point ( $t = 624$  sec) after which it may start getting rubbed off. As a result, the PNC starts increasing gradually. It attains the same value as for the other nanocoating or the reference towards the end of the abrasion. The standard deviation in the values measured for the nanocoating with PMMA varies from 0.7 to  $27 \text{ cm}^{-3}$ .

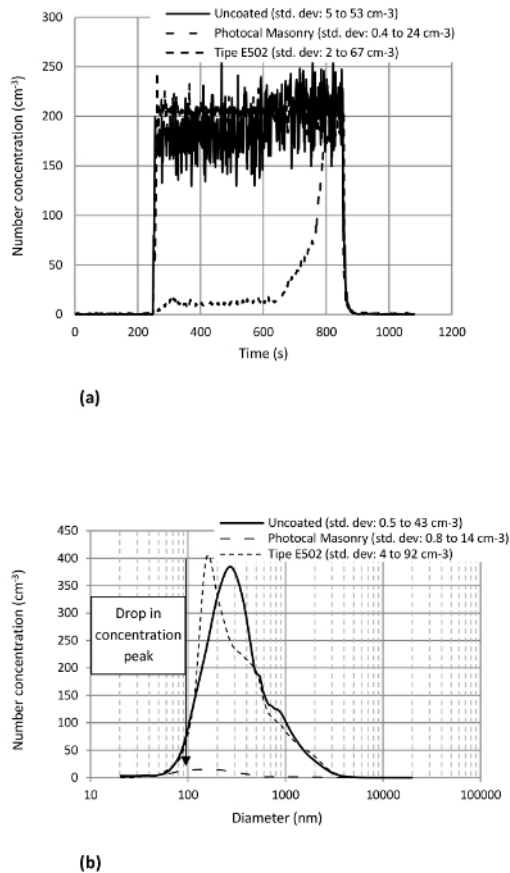
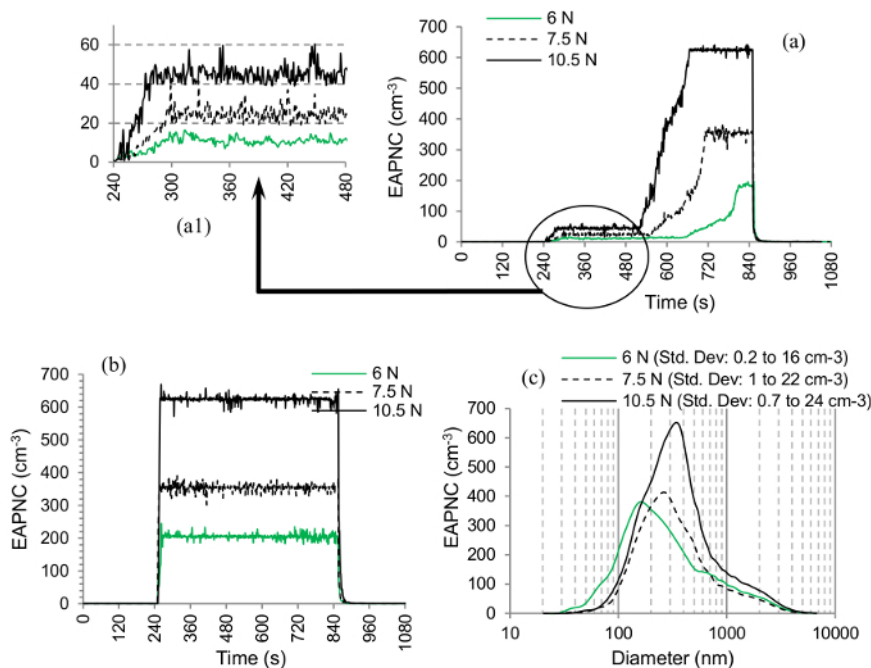


**Figure 10. Effect of the Nanocoating Types on the Aerosol Particles Generation from the Nanocoatings. (A)** PNC variation with time **(B)** PSD of the aerosol particles emitted during the abrasion of 4 layers of the nanocoating under 6 N of normal load (note: all the curves are mean curves obtained from 3 repeated tests) (Shandilya *et al.*<sup>33</sup>) [Please click here to view a larger version of this figure.](#)

In **Figure 10B**, the PSD of the emitted aerosol particles is shown. The nanocoating with alcoholic base seems to have no effect on the PSD either except the shift of the size mode towards smaller particle sizes ( $154 \pm 10$  nm). The standard deviation in the PSD measured in this case changes from 0.2 to 16 cm<sup>-3</sup>. The nanocoating with PMMA considerably drops the peak of the PSD curve by a factor of # 30 rendering the particle emission totally insignificant. The standard deviation measured here is 8 cm<sup>-3</sup> maximum.

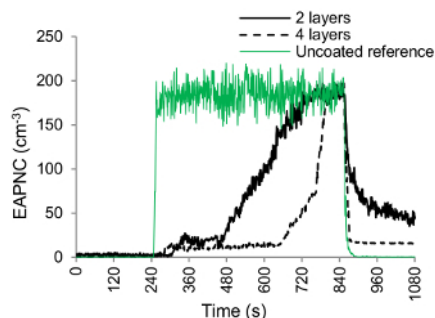
In **Figure 11A**, effect of increasing  $F_N$  has been shown on a 4 layered nanocoating with PMMA. The abrasion commences at  $t = 240$  sec and ends at  $t = 840$  sec. For a clear view of the PNC, between  $t = 240$  sec and  $t = 480$  sec, a zoomed view in **Figure 11A1** is also shown. The PNC increases with normal load. The same pattern continues in **Figure 11B** for a 4 layered nanocoating with the alcoholic base too. While measuring the PSD for the nanocoating with PMMA, the PSD showed very low concentrations which were even close to their particle detection thresholds. Hence, the two particle sizers were not employed further. But for the nanocoating with alcoholic base, there were no such problems. The PSD in this case is shown in **Figure 11C**. Three unimodal distributions with increasing size modes (*i.e.*, 154 nm to 274 nm to 365 nm) and increasing concentration peaks can be seen for increasing normal loads.





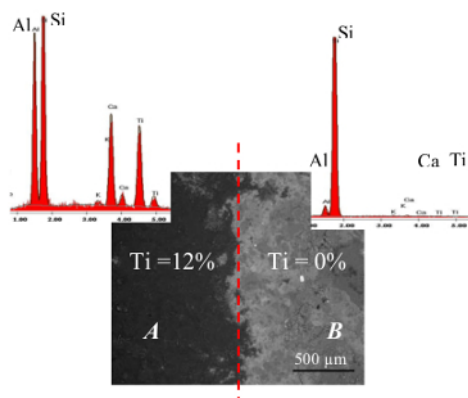
**Figure 11. Effect of the Normal Load on the Aerosol Particles Generation from the Nanocoatings.** (A) PNC variation with time for 4 layers of nanocoating with PMMA and (B) alcoholic base; (a1) zoomed view; (C) PSD of the aerosol particles emitted during the abrasion of 4 layers of nanocoating with alcoholic base (note: all the curves are mean curves obtained from 3 repeated tests) (Shandilya *et al.*<sup>33</sup>) [Please click here to view a larger version of this figure.](#)

The number of layers also has a substantial effect on PNC. The **Figure 12** demonstrates this effect where two samples, having 2 and 4 layers of the nanocoating with PMMA, are tested for  $F_N = 6$  N. The abrasion commences at  $t = 240$  sec and ends at  $t = 840$  sec. The PNC is always lower when 4 layers of the nanocoating (std. deviation: 2 to 27 cm<sup>-3</sup>) is abraded as compared to the 2 layers (std. deviation: 13 to 37 cm<sup>-3</sup>) or an uncoated reference. Both sets of layers seem to provide resistance towards abrasion. However, in the case of the nanocoating with alcoholic base, both 2 and 4 layers have similar PNC.



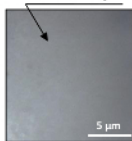
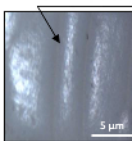
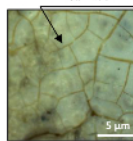
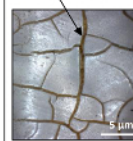
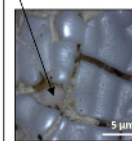
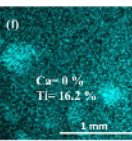
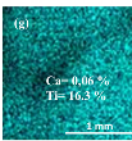
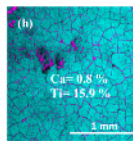
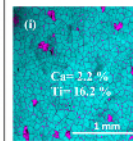
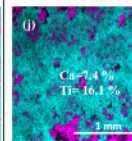
**Figure 12. Effect of the Number of Coating Layers on the Aerosol Particles Generation from the Nano-coatings.** PNC variation with time for 2 and 4 layers of nanocoating with PMMA (note: all the curves are mean curves obtained from 3 repeated tests) (Shandilya *et al.*<sup>33</sup>) [Please click here to view a larger version of this figure.](#)

The SEM observations of the 4 layered nanocoating with PMMA were also done at the end of the abrasion. The **Figure 13** shows the observation. An unabraded coated surface (marked A) had an average Ti content of # 12% (in mass). For the abraded part (marked B), the average Ti content lowers down to # 0% (in mass), thus, completely exposing the brick surface.



**Figure 13. Microscopic Analysis of the Nanocoated Surfaces.** SEM image and EDX analysis of the coated and abraded parts of the nanocoating with PMMA; part (A): unabraded coated surface; part (B): abraded (Shandilya *et al.*<sup>33</sup>) [Please click here to view a larger version of this figure.](#)

Hence, a 4 layered nanocoating with PMMA has performed remarkably well as compared to its 2 layered counterpart or the other nanocoating, including its both 2 and 4 layers of nanocoating. Considering this observation, some 4 layered samples of the nanocoating with PMMA were also exposed to the artificial accelerated weathering prior to their abrasion. In **Figures 14A-E**, one may see a deteriorating effect of the weathering. A continuous and integrated form of the nonweathered nanocoating can be observed in **Figure 14A**. A progressive deterioration of the nanocoating via cracking can be then observed in the successive figures *i.e.*, **Figures 14B, C, D and E**. On the contrary, an uncoated reference shows no such effects. The drying stress due to water content evaporation and gradual embrittlement of the polymeric binder present in the nanocoating during its interaction with UV rays result in such a deterioration (White<sup>35</sup>, Murray<sup>36</sup>, Dufresne *et al.*<sup>37</sup>, Hare<sup>38</sup> Tirumkudulu and Russel<sup>39</sup>). The EDS analysis of the weathered nanocoating via elemental mapping between Ti (contributed by the nanocoating) and Ca (contributed by the brick) is shown in **Figures 14F-J**. In the figure, an almost stagnant Ti content on the surface (average value #16.1%) can be observed with an increasing Ca content and hence the exposed surface. One of the major implications of this result can be the shrinkage of nanocoating with weathering.

	No weathering	2 months of weathering	4 months of weathering	6 months of weathering	7 months of weathering
Optical Microscopy of the nanocoated test samples	(a) Continuous and intact form of the nanocoating 	(b) Ridge and valley formation on the nanocoated surface 	(c) Cracking of the nanocoated surface 	(d) Crack broadening 	(e) Lump formation 
Spatial distribution mapping of Ca and Ti over nanocoated test samples	(f) Ca=0.0% Ti=16.2% 	(g) Ca=0.06% Ti=16.3% 	(h) Ca=0.8% Ti=15.9% 	(i) Ca=2.2% Ti=16.2% 	(j) Ca=1.4% Ti=16.1% 
	Nanocoating deposited all over the surface	No effect; Exposed surface = 0.1 mm <sup>2</sup>	Brick exposure through cracks; Exposed surface = 0.53 mm <sup>2</sup>	Exposed surface = 1.19 mm <sup>2</sup>	Exposed surface = 2.83 mm <sup>2</sup>

**Figure 14. Microscopic Analysis of Progressively Deteriorating Nanocoating (Shandilya *et al.*<sup>31</sup>).** The deterioration is via the appearance of cracks on the surface which deepens up with time [Please click here to view a larger version of this figure.](#)

The quantification of the TiO<sub>2</sub> nanoparticles emission in the water was carried out at the intervals of 2, 4, 6 and 7 months of weathering. For this 100 ml samples of leachate were taken from the collected runoff water and analyzed using an Inductively Coupled Plasma Mass Spectrometry (ICP-MS). **Table 3** shows ICP-MS's operating conditions. We found that the Ti was found to be always below the threshold detection value (= 0.5 μg/l) in the sample volume. This observation leads to the conclusion that despite the deterioration by weathering, the nanocoating is still strongly bound to resist their leaching into the runoff waters.

Sample volume	2 ml
RF Power	1550 W
RF Matching	1.78 V
Carrier Gas	0.85 l/min
Makeup gas	0.2 l/min
Nebulizer	Micromist
Nebulizer pump	0.1 r/s
S/C temperature	15 °C
He flow rate	5 ml/min
H <sub>2</sub> flow rate	2 ml/min
Integration time	0.1 s
Chamber & Torch	Quartz
Cone	Ni

**Table 3: Operating Conditions of ICP-MS.**

The weathering was followed by the abrasion. The **Figures 15A and B** show the results of TEM analysis of the sampled aerosol particles, during the first 2 min of abrasion of the 4 and 7 months weathered nanocoating under the same sampling conditions. A qualitatively higher deposition of aerosol particles on the mesh grids can be observed in the case of latter. The polydispersed aerosol particles can be observed upon higher magnification. Even though we weren't able to quantify, but a significant amount of free nanoparticles of TiO<sub>2</sub> (*i.e.*, Ti mass > 90%) was observed when 7 months weathered nanocoating was abraded (**Figure 15C and D**). Confidence intervals are small to the measured quantities and thus neglected in the plots. This result differs from the findings of non-weathered nanocoatings and various other studies like Shandilya *et al.*<sup>15</sup>, Golanski *et al.*<sup>23</sup>, Göhler *et al.*<sup>29</sup>, Shandilya *et al.*<sup>33</sup>. Hence, it is of more particular interest. In previously obtained results for non-weathered nanocoatings and other mentioned studies, a large fraction of the emitted aerosols composed of the nanomaterial in the matrix-bound state and not in the free state.

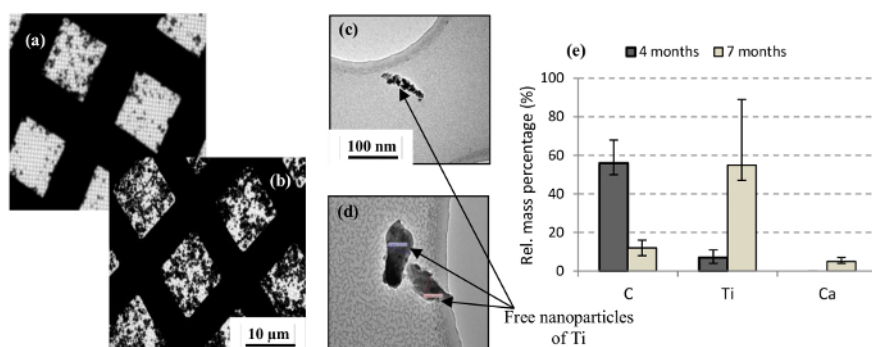
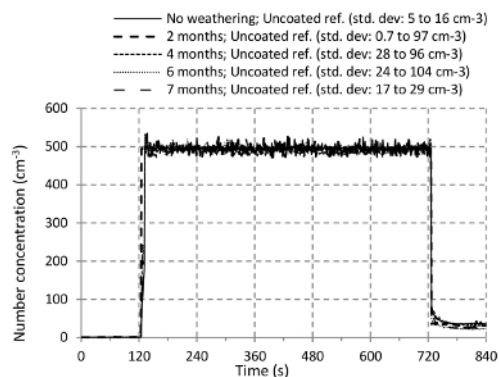
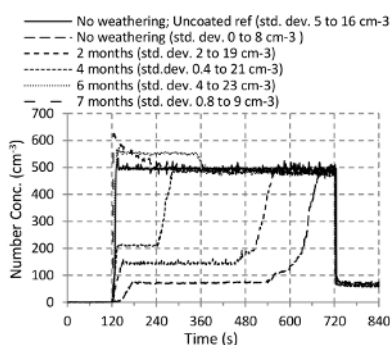


**Figure 15. Microscopic Analysis of the Aerosol Particles.** TEM image of aerosol particles emitted from the abrasion of **(A)** 4 months and **(B)** 7 months weathered nanocoating **(C, D)** free nanoparticles emitted from the abrasion of 7 months weathered nanocoating **(E)** Chemical analysis of aerosol particles emitted from the abrasion of 4 and 7 months weathered nanocoating (Shandilya *et al.*<sup>31</sup>) [Please click here to view a larger version of this figure.](#)

In the **Figure 15E**, the variations in the percentages of the three elements- C, Ti and Ca are shown when the weathering duration reaches 7 months from 4 months. A clear effect of the polymer embrittlement can be observed with a drop in the C content from 56% to 12%. This drop directly implies the reduction in the presence of the matrix around the emitted aerosol particles. An increase from 7% to 55% in the Ti content signifies an increase of Ti concentration in the emitted aerosol particles. The exposed surface of the underlying brick, after 7 months of weathering, yields some aerosol particles too upon abrasion. As a result, some aerosol particles from the brick are also observed after 7 months of weathering. Hence, the weathering duration has a direct impact on the size and chemical composition of the aerosol particles.



(a)



(b)

**Figure 16. PNC and PSD as a Function of the Abrasion Duration:** PNC and PSD during the abrasion of weathered reference and nanocoating. The abrasion takes place for  $t = 120$ – $720$  sec in panels (A) and (B). (Shandilya *et al.*<sup>31</sup>) [Please click here to view a larger version of this figure.](#)

The **Figures 16A–D** show the results on PNC and PSD of the aerosol particles sampled within the volume of the sampling hood. In **Figures 16A** and **B**, starting at  $t = 120$  sec and continuing until  $t = 720$  sec, the abrasion of the uncoated reference yielded a constant and weathering duration independent PNC ( $\approx 500 \text{ cm}^{-3}$ ; standard deviation  $5 - 16 \text{ cm}^{-3}$ ; repeated thrice). Therefore, the artificial weathering has no apparent effect on emitted aerosol particles from the uncoated reference. However, in the case of the nanocoating, a clear effect of the weathering duration can be observed as the PNC increases with weathering duration. Except for 6 and 7 months, the nature of its variation with time is also strikingly similar *i.e.*, initial ascension, followed by stagnation, then ascension again, and the final stagnation. For 6 and 7 months, there is an immediate bump in the concentration as soon as the abrasion starts. This initial bump in the concentration is even higher than that of the reference. However, after  $t = 360$  sec, it tends to come back to the reference level. This difference in the nanocoating behavior with respect to the abrasion can be explained on the basis of its removal mechanism during abrasion. Until 4 months of the weathering, the nanocoating is believed to be strong enough to resist its abrasion. As a result, it gets *worn* slowly and hence, the number concentration of the emitted aerosols increases slowly. However, after 6 and 7 months of the weathering, the nanocoating is lumpy (as already seen in the **Figure 14E**) as possibly loosely attached to the brick's surface. As a result, as soon as the abrasion starts, these nanocoating lumps get *uprooted* easily which shows a bump in the number concentration of the emitted aerosol particles. The PSD of the emitted aerosol particles for the reference (**Figure 16C**) shows no apparent effect of the weathering (mode alternating between 250 and 350 nm;  $\text{PNC} \approx 375 \text{ cm}^{-3}$ ; standard deviation  $0.2 - 8 \text{ cm}^{-3}$ ). In **Figure 16D**, the particle size distribution is shown for the nanocoating that correspond to the first phase during which the PNC is stagnant. This figure does not show any curve for 6 and 7 months weathering because there is no first stagnant phase for them. As one may see clearly, there is an increase in the size mode as well as maximum PNC.

#### Emission from the Glaze

Contrary to the aerosol particles emission observations in the case of the reinforced bricks and photocatalytic nanocoatings, the two layers of glaze were found to be non-emissive during their abrasion when  $F_N = 6 \text{ N}$ . The number concentration of the emitted aerosol particles, obtained using the particle counter, was always found to be less than  $1 \text{ cm}^{-3}$ , hence insignificant.

## Discussion

In the present article, an experimental investigation of the nanosafety-by-design of commercial nanostructured products is presented. The nanosafety-by-design of any product can be studied in terms of its PNC and PSD when it is subjected to mechanical stresses and environmental weathering. The products chosen for the study are alumino-silicate brick reinforced with  $\text{TiO}_2$  nanoparticles, glaze with  $\text{CeO}_2$  nanoparticles and

photocatalytic nanocoatings with TiO<sub>2</sub> nanoparticles. These products are easily accessible to the customers in the commercial market and well associated with their daily lives. Therefore, their investigation towards their nanosafety-by-design is crucial.

### Artificial Weathering

Variation in degradation observations may be expected when different operating conditions are used. Moreover, the spectral power distribution of light from fluorescent UV/xenon arc lamps is significantly different from that produced in light and water exposure devices using other light sources. The type and rate of degradation and the performance rankings produced in exposures to UV lamps can be much different from those produced by exposures to other types of laboratory light sources. The weathering test results also depend upon the care that is taken to operate the weathering chamber. Hence, the factors like the regulation of line voltage, temperature of the room in which the device operates, temperature controls, and condition and age of the lamps do also play a significant role in the performance of the weathering chamber. During testing, the irradiance may change due to ageing of the UV lamp. A standard lamp has an average life of  $\approx 1,400$  hr. Therefore, before starting the weathering test, one should make sure of the number of hours left for the lamp to run. The presence of metallic ions in the water to be sprayed inside the weathering chamber which increase its conductivity is also an important aspect to take care of. If the water conductivity exceeds the acceptable level, it may leave the traces of the dissolved metals on the weathered surface. In such cases, a more degraded surface is obtained than expected. The distribution of the irradiance from the UV lamp is sometimes not uniform all over the stainless steel support over which the nanocoating samples are placed. In such a case, care should be taken during the placement of the nanocoating samples so that an individual variation in the irradiance level on the surface of each sample does not exceed  $\pm 2 \text{ W/m}^2$ . To allow the reproducibility of the weathering results, at least three replicates of each material must be exposed.

### Abrasion and ENM Aerosols Characterization

The particles number concentration varies with the placement of the sampling point of the aerosol particles inside the emission test chamber as the concentration is not uniform throughout the chamber. In the present study, the sampling point has been kept near to the surface being abraded. This allows the minimization of the diffusion and sedimentation losses of the aerosol particles as they are sampled as soon as they get generated from the abrasion. The flow rate of the particle free air is also critical as it should be high enough to reduce the background particles to their minimum concentration so that they do not interfere with the characterization of the abrasion generated particles. During abrasion, the edge chamfered abradant allows the abrasion to be uniform inside its contact area with the nanostructured product. If the edges are not chamfered properly, they might peel off the contact surface too. While working with the nanostructured products, an operator is highly susceptible to his/her exposure to the emitted nanoparticles. Hence, any kind of manipulation of the nanostructured products, including abrasion, must be carried out inside a closed conformity which is able to impede any nanoparticle to pass through.

### TEM Analysis of the Liquid Suspension

The hydrophilic nature of the copper mesh grid is of utmost importance while depositing as aqueous base drop. It stabilizes the drop on the grid's surface as well as alleviates the need of surface pre-wetting operations. The drying of the charged grid inside the closed chamber is also critical to avoid its contamination with the ambient dirt particles as they may interfere with the TEM analysis.

The standard abrasion apparatus has been modified by replacing the already installed horizontal steel bar by a replica in aluminum 2024 alloy and mounting a strain gauge on the top surface of this replicated aluminum alloy bar. This modification allows knowing the complete mechanical stress state during abrasion and hence better control of the process, which was not possible earlier. For the microscopic analysis of aerosol particles, a new particle collection technique based on filtration through TEM-dedicated supports, namely TEM porous grids has been employed in the present study through a filter holder which has been developed specifically for this application.

### Artificial Weathering

The ability of a coating to resist deterioration of its physical properties caused by exposure to light, heat, and water can be very significant for many applications. The type of the exposure presented in this article is limited and cannot simulate the deterioration caused by localized weather phenomena such as atmospheric pollution, biological attack, or saltwater exposure.

### Abrasion and ENM Aerosols Characterization

A major limitation of the protocol presented for the ENM aerosols characterization is that a fraction of these ENM aerosols get lost before they can be characterized for their size and number. Such a loss can be attributed to various phenomena associated with the aerosol dynamics like sedimentation, diffusion, turbulence in the air flow, inertial deposition etc. which act on an aerosol particle simultaneously as soon as it gets emitted. This loss is a direct function of the aerosol particle size. This aspect has been considered in some previous publications like Shandilya *et al.*<sup>31</sup>, Shandilya *et al.*<sup>33</sup>, Shandilya *et al.*<sup>34</sup>. However, the consideration approach has been reactive in these studies *i.e.*, calculations were done to approximately estimate the loss and the final experimental results were modified on the basis of the calculation results.

### TEM Analysis of the Liquid Suspension

The technique presented here for the TEM analysis of a diluted sampled liquid suspension forces the suspended particles to adhere to the surface of the grid by evaporating the total water content. This may allow the formation of bigger aggregates on the grid which are not present in the original liquid suspension. Hence, this technique cannot completely represent the morphology of the suspended particles in the original conditions.

The technique presented here aims at controlling the parameters which play a key role in particles aerosolization, whether it is during mechanical or environmental ageing. Moreover, it focuses on finding a weathering duration threshold beyond which the chosen nanocoating has exceeded its nanosafe lifetime. (In the present case, it's 4 months of accelerated weathering.) This is done through a continuous monitoring of the in-process nanocoating state which allowed us to note the exact duration in which the nanocoating started to deteriorate. This is the feature which distinguishes it from previous scientific studies as they deal with the concept of the environmental weathering by applying it on a test sample for a predetermined duration with no in-process monitoring of the ongoing weathering. The approach chosen in the study presented here allows for quantitatively comparing experimentally measured nanosafety thresholds (*i.e.*, nanosafe lifetimes) of different -but similar- nanoproductions<sup>42</sup> (under similar accelerated life conditions). It is thus the first step developing products on a Nanosafety-by-design basis.



For the future, a completely preemptive approach is being developed in which the experimental set-up minimizes the aerosol particle losses in the real time and a complete quantitative study of the emitted aerosol particles can be done with accuracy.

## Disclosures

The authors have nothing to disclose.

## Acknowledgements

This work was carried out in the framework of the Labex SERENADE (ANR-11-LABX-0064) and the A\*MIDEX Project (ANR-11-IDEX-0001-02), funded by the French Government program, Investissements d'Avenir, and managed by the French National Research Agency (ANR). We thank the French Ministry of Environment (DRC 33 and Program 190) and ANSES (Nanodata Project 2012/2/154, APR ANSES 2012) for financing the work. We are equally grateful to Olivier Aguerre-Chariol, Patrice Delalain, Morgane Dalle, Laurent Meunier, Pauline Molina, and Farid Ait-Ben-Ahmad for their cooperation and advice during the experiments.

## References

- Potocnick, J. *European Commission Recommendation on the definition of nanomaterial (2011/696/EU)*. (2011).
- Oberdorster, G., Oberdorster, E., Oberdorster, J. Nanotoxicology: an emerging discipline evolving from studies of ultrafine particles. *Environ Health Persp.* **113** (7), 823-839 (2005).
- Le Bihan, O., Shandilya, N., Gheerardyn, L., Guillon, O., Dore, E., Morgeneyer, M. Investigation of the Release of Particles from a Nanocoated Product. *Adv Nanoparticles.* **2** (1), 39-44, (2013).
- Houdy, P., Lahmani, M., Marano, F. *Nanoethics and Nanotoxicology. 1st ed.* Springer, Heidelberg, Germany (2011).
- Kulkarni, P., Baron, P. A., Willeke, K. *Aerosol Measurement: Principle, Techniques and Applications. 3rd ed.* John Wiley and Sons, Hoboken, NJ, USA (2011).
- Hsu, L.Y., Chein, H.M. Evaluation of nanoparticle emission for TiO<sub>2</sub> nanopowder coating materials. *J Nanopart Res.* **9** (1), 157-163 (2007).
- Maynard, A.D. Safe handling of nanotechnology. *Nature.* **444** (1), 267-269 (2006).
- Shatkin, J.A. *et al.* Nano risk analysis: advancing the science for nanomaterials risk management. *Risk Anal.* **30** (11), 1680-1687 (2011).
- Göhler, D., Nogowski, A., Fiala, P., Stintz, M. Nanoparticle release from nanocomposites due to mechanical treatment at two stages of the life-cycle. *Phys Conf Ser.* **429** 012045 (2013).
- Allen, N.S. *et al.* Ageing and stabilisation of filled polymers: an overview. *Polym Degrad Stabil.* **61** (2), 183-199 (2004).
- Allen, N.S. *et al.* Degradation and stabilisation of polymers and coatings: nano versus pigmentary titania particles. *Polym Degrad Stabil.* **85** (3), 927-946 (2004).
- Al-Kattan, A. *et al.* Release of TiO<sub>2</sub> from paints containing pigment-TiO<sub>2</sub> or nano-TiO<sub>2</sub> by weathering. *J Environ Monitor.* **15** (12), 2186-2193 (2013).
- Kaegi, R. *et al.* Synthetic TiO<sub>2</sub> nanoparticle emission from exterior facades into the aquatic environment. *Environ Pollut.* **156** (2), 233- 239 (2008).
- Hirth, S., Cena, L., Cox, G., Tomovic, Z., Peters, T., Wohlleben, W. Scenarios and methods that induce protruding or released CNTs after degradation of nanocomposite materials. *J Nanopart Res.* **15** (2), 1504-1518 (2013).
- Shandilya, N., Le Bihan, O., Morgeneyer, M. A review on the study of the generation of (nano-) particles aerosols during the mechanical solicitation of materials. *J Nanomater.* **2014**, 289108 (2014).
- Wohlleben, W. *et al.* On the lifecycle of nanocomposites: comparing released fragments and their *in vivo* hazards from three release mechanisms and four nanocomposites. *Small.* **7** (16), 2384-2395 (2011).
- Bouillard, J. X. *et al.* Nanosafety by design: risks from nanocomposite/nano waste combustion. *J Nanopart Res.* **15** (1), 1519-1529 (2013).
- Ounoughene, G. *et al.* Behavior and fate of Halloysite Nanotubes (HNTs) when incinerating PA6/HNTs nanocomposite. *Environ Sci Technol.* **49** (9), 5450-5457 (2015).
- Morose, G. The 5 principles of "Design for Safer Nanotechnology". *J Clean Prod.* **18** (3), 285-289 (2010).
- ASTM International, *Standard test method for the abrasion of organic coatings by the Taber abrader.* **ASTM D4060**, (2007).
- ASTM International, *Standard test methods for dry abrasion mar resistance of high gloss coatings.* **ASTM D6037**, (1996).
- ASTM International, *Standard test method for resistance of transparent plastics to surface abrasion.* **ASTM D1044**, (2008).
- Golanski, L., Guiot, A., Pras, M., Malarde, M., Tardif, F. Release-ability of nano fillers from different nanomaterials (toward the acceptability of nanoproduit). *J Nanopart Res.* **14** (1), 962-970 (2012).
- Vorbau, M., Hillemann, L., Stintz, M. Method for the characterization of the abrasion induced nanoparticle release into air from surface coatings. *J Aerosol Sci.* **40** (3), 209-217 (2009).
- Hassan, M.M., Dylla, H., Mohammad, L.N., Rupnow, T. Evaluation of the durability of titanium dioxide photocatalyst coating for concrete pavement. *Constr Build Mater.* **24** (8), 1456-1461 (2010).
- Morgeneyer, M., Shandilya, N., Chen, Y.M., Le Bihan, O. Use of a modified Taber abrasion apparatus for investigating the complete stress state during abrasion and in-process wear particle aerosol generation. *Chem Eng Res Des.* **93** (1), 251-256 (2015).
- Morgeneyer, M., Le Bihan, O., Ustache, A., Aguerre Chariol, O. Experimental study of the aerosolization of fine alumina particles from bulk by a vortex shaker. *Powder Technol.* **246** (1), 583-589 (2013).
- Le Bihan, O., Morgeneyer, M., Shandilya, N., Aguerre Chariol, O., Bressot, C. Chapt. 7, In *Handbook of Nanosafety: Measurement, Exposure and Toxicology*. (Eds.) Vogel, U., Savolainen, K., Wu, Q., Van Tongeren, M., Brouwer, D., Berges, M. Academic Press, San Diego, CA. (2014).
- Göhler, D., Stintz, M., Hillemann, L., Vorbau, M. Characterization of nanoparticle release from surface coatings by the simulation of a sanding process. *Ann Occup Hyg.* **54** (6), 615-624 (2010).
- R'mili, B., Le Bihan, O., Dutouquet, C., Aguerre Chariol, O., Frejafon, E. Sampling by TEM grid filtration. *Aerosol Sci Tech.* **47** (7), 767-775 (2013).

31. Shandilya, N., Le Bihan, O., Bressot, C., Morgeneier, M. Emission of Titanium Dioxide Nanoparticles from Building Materials to the Environment by Wear and Weather. *Environ Sci Technol.* **49** (4), 2163–2170 (2015).
32. AFNOR. *Paints and varnishes – Methods of exposure to laboratory light sources – Part 1: General guidance.* **ISO 16474-1**, (2012).
33. Shandilya, N., Le Bihan, O., Bressot, C., Morgeneier, M. Evaluation of the particle aerosolization from n-TiO<sub>2</sub> photocatalytic nanocoatings under abrasion, *J Nanomater.* **2014**, 185080 (2014).
34. Shandilya, N., Le Bihan, O., Morgeneier, M. Effect of the Normal Load on the release of aerosol wear particles during abrasion. *Tribol Lett.* **55** (2), 227–234 (2014).
35. White, L. R. Capillary rise in powders. *J Colloid Interf Sci.* **90** (2), 536–538 (1982).
36. Murray, M. *Cracking in coatings from colloidal dispersions: An industrial perspective.* Proceedings Rideal Lecture, London, April 20. <<http://www.soci.org/~media/Files/Conference%20Downloads/2009/Rideal%20Lectures%20Apr%2009/Murray.ashx>> (2009).
37. Dufresne, E.R. *et al.* Flow and fracture in drying nanoparticle suspensions, *Phys Rev Lett.* **91**, 224501 (2003).
38. Hare, C.H. *The degradation of coatings by ultraviolet light and electromagnetic radiation.* JPCL. <<http://www.q-lab.com/documents/public/70ccb209-bf41-4da0-bb80-964d597fc728.pdf>> (1992).
39. Tirumkudulu, M.S., Russel, W.B. Cracking in drying latex films, *Langmuir.* **21** (11), 4938–4948 (2005).
40. Shandilya, N., Morgeneier, M., Le Bihan, O. First development to model aerosol emission from solid surfaces subjected to mechanical stresses: I. Development and results. *J Aerosol Sci.* **89**, 43–57 (2015).
41. Shandilya, N., Morgeneier, M., Le Bihan, O. First development to model aerosol emission from solid surfaces subjected to mechanical stresses: II. Experiment-Theory comparison, simulation and sensibility analysis. *J Aerosol Sci.* **89**, 1–17 (2015).
42. Bressot, C., *et al.* Environmental release of engineered nanomaterials from commercial tiles under standardized abrasion conditions. *J Hazardous Materials.* (2016).